SnTe$_x$Se$_{1-x}$ Alloy: An Effective Alternative to SnSe Nano-crystalline Thin Films for Optoelectronic Applications

ANJALI DEVI,[1] ARUN BANOTRA,[1] SHIV KUMAR,[2] ASHOK K. KAPOOR,[2] and NARESH PADHA [1,3]

1.—Department of Physics, University of Jammu, Jammu, J&K 180006, India. 2.—Solid State Physics Laboratory, DRDO, Timarpur, New Delhi 110054, India. 3.—e-mail: nareshpadha@gmail.com

As prepared by fusion, SnTe$_x$Se$_{1-x}$ ($x = 0.68$) alloy is found to possess mixed phases of hexagonal Te and orthorhombic SnSe. The deposited films of this alloy demonstrate incongruent evaporation of the constituents. Reductions in c-parameter and strain along the z-axis in lattices of SnSe and Te constituents have been observed in these films at 353 K. These deviations in the structure of SnTe$_x$Se$_{1-x}$ films make it superior to SnSe for various optoelectronic applications. The absorption coefficient of SnTe$_x$Se$_{1-x}$ films is higher than SnSe, and its bandgap attains a value of 0.93 eV. Further, resistivity value of SnTe$_x$Se$_{1-x}$ ($\sim 6.12 \times 10^{-2}$ Ω cm) is lower and carrier concentration ($\sim 1.31 \times 10^{19}$ cm^{-3}) is higher than SnSe, whereas its mobility value (~ 25.8 cm^2/V s) matches SnSe and similar materials. The surface quality of SnTe$_x$Se$_{1-x}$ improves and number of crystallites increases. The interface of p-SnTe$_x$Se$_{1-x}$ with Ag metal forms a Schottky diode. The current–voltage (I–V) behaviour of Ag/p-SnTe$_x$Se$_{1-x}$ Schottky diodes is analysed and diode parameters are determined by using thermionic emission and diffusion (TED) current transport mechanism.

Key words: SnTe$_x$Se$_{1-x}$ alloy, lattice strain, absorption coefficient, bandgap, resistivity, Schottky diode

INTRODUCTION

Metal chalcogenides and their solid solutions have become materials of considerable interest because of their applications in energy conversion devices and infrared (IR) generation and detection systems.[1–4] Their exceptional properties with respect to their chemical composition and nanoscale dimension reveal a variety of fascinating attributes, which provide solutions to a variety of issues.[5,6] Recently, much attention has been paid to the physical properties of layered tin mono-chalcogenide (SnSe, SnS and SnTe) semiconductors.[7] These are small bandgap semiconductors that have been of great interest due to their thermodynamic, vibrational and electronic properties. A number of attempts have been made by different researchers to investigate the electrical and optical properties of thin films of these materials.[8] Tin selenide (SnSe) having direct energy bandgap ($E_g \sim 1.24$ eV) and absorption coefficient ($\alpha \geq 10^4$ cm^{-1}) has been used as an efficient absorber layer in the solar cell structure.[9] The SnTe$_x$Se$_{1-x}$ ($0 \leq x \leq 1$) semiconductor alloy based thin films show variation in their energy bandgap (E_g) due to change in composition and, thus, absorbs different regions of E. M. spectrum.[10] Moreover, these films are reported to display peculiarities in the band structure and behave an interesting object for applied as well as fundamental research.[9] The SnTe$_x$Se$_{1-x}$ solid solutions are reported to be formed on mixing of SnSe (orthorhombic) and SnTe (cubic) compounds.[10–12] The continuous variation of E_g and lattice constants observed with change in composition of SnTe$_x$Se$_{1-x}$

is of significant importance.[10] In the present work, $SnTe_xSe_{1-x}$ thin films are seen to possess mixed phases of Te (hexagonal) and SnSe (orthorhombic) crystallites. Their behaviour as a function of changing Te and SnSe constituents has been investigated. Finally, Ag/p-$SnTe_xSe_{1-x}$ Schottky diodes of different areas were fabricated on indium doped tin oxide (ITO) substrate and their (I–V) characteristics analysed.

EXPERIMENTAL

The $SnTe_xSe_{1-x}$ alloy has been synthesised by direct fusion of the highly pure (purity 99.999%) elements of Sn, Se and Te in a vacuum sealed tube at high temperatures. The obtained solid ingot was powdered to a mean particle size ~ 100 μm using grinding and sieving. The details of processing have been reported by Padha et al.[13] The 400 nm thick films of $SnTe_xSe_{1-x}$, Te and SnSe were deposited on ultrasonically cleaned Corning glass substrates at 353 K; the films of $SnTe_xSe_{1-x}$ were also deposited at 300 K. The thickness and the deposition rate of the films were measured from digital thickness monitor (Make: HindiVac, India; Model: DTM-101) fitted in the vacuum coating unit (VCU). The x-ray diffraction data of the $SnTe_xSe_{1-x}$, Te, and SnSe powders and thin films were recorded using an x-ray diffractometer (Make: PANalytical; Model: Xpert[3]) in the 2θ range of 10° to 70° with a scan speed 0.05 °/s. The morphology of these samples was determined by using scanning electron microscopy (SEM) (Make: ZEISS; Model: SUPRA-55). The compositions of the $SnTe_xSe_{1-x}$ powder and thin films were determined from the energy dispersive x-ray analysis (EDAX) attachment of SEM (Make: OXFORD; Model: 7426). The transmission and absorbance spectra of the deposited films were measured by using UV–Vis-NIR spectrophotometry (Make: Shimadzu; Model: UV 3600) in the wavelength range 750 nm to 2250 nm. The electrical characteristics of the samples were obtained by using a Hall measurement setup (Make: BioRad; Model: HL-5200). The samples of $SnTe_xSe_{1-x}$ of 1×1 cm^2 area and thickness 600 nm deposited over indium-doped tin oxide (ITO) coated glass substrate were inserted into the deposition chamber immediately. The ITO coating was used as the back ohmic contact. The Schottky contacts were formed over the $SnTe_xSe_{1-x}$ top surface by evaporating 160 nm thick silver (Ag, 99.999%) as dots with diameters of about 1.0 mm, 1.5 mm and 2.0 mm. The I–V measurements were performed by the use of Keithely 2400 source meter. The Schottky diodes showing identical current–voltage (I–V) characteristics were selected for the measurement of diode parameters. All calculations were performed by using Origin software (Make: Microcal Software, Inc. Northampton, MA, USA; Model: Version 6.1). All depositions in the vacuum coating unit (VCU) were undertaken at a base pressure of 2×10^{-6} mbar.

RESULTS AND DISCUSSION

Structural Analysis of $SnTe_xSe_{1-x}$ Powder and Thin Films

The x-ray diffraction patterns of powder materials of Te, $SnTe_xSe_{1-x}$ and SnSe are shown in Fig. 1. The $SnTe_xSe_{1-x}$ powder is found to possess mixed phases of SnSe (orthorhombic) and Te (hexagonal) crystallites. The peaks emerge at $2\theta = 27.607(1)°$, $38.368(3)°$, $40.477(3)°$ correspond to the (101), (012), (110) set of planes of Te with space group P31 2 1 (JCPDS card no. 89-4899), while those occuring at $2\theta = 30.393(2)°$, $31.041(8)°$, $37.720(4)°$ represent (400), (111), (311) diffraction planes of SnSe with space group Pnma (JCPDS card no. 48-1224). SnSe (400) planes occupy the highest intensity peak, while the second highest peak is represented by Te (101) planes. The presence of an additional (001) $SnSe_2$ peak is also observed in $SnTe_xSe_{1-x}$ and SnSe powders (JCPDS Card No 23-0602).

The $SnTe_xSe_{1-x}$, SnSe and Te powders are deposited on corning glass substrates at 353 K in a vacuum coating unit (VCU) to obtain thin films of 400 nm thicknesses, the films of $SnTe_xSe_{1-x}$ were also deposited at 300 K. Figure 2 shows x-ray diffraction patterns of $SnTe_xSe_{1-x}$ powder, as well as films deposited at 300 K and 353 K. The x-ray diffraction data of the films deposited at 300 K exhibit high intensity Te peaks alongwith some low intensity SnSe peaks. However, the films deposited at 353 K show an increase in the intensity of Te and SnSe peaks to that deposited at 300 K. These films exhibit incongruent evaporation of the constituent Te and SnSe due to vapour pressure difference between the two. Figure 3 shows x-ray diffraction patterns of thin films of Te, $SnTe_xSe_{1-x}$ and SnSe each deposited at 353 K. The unit cell parameters of Te and SnSe constituents of $SnTe_xSe_{1-x}$ powder and

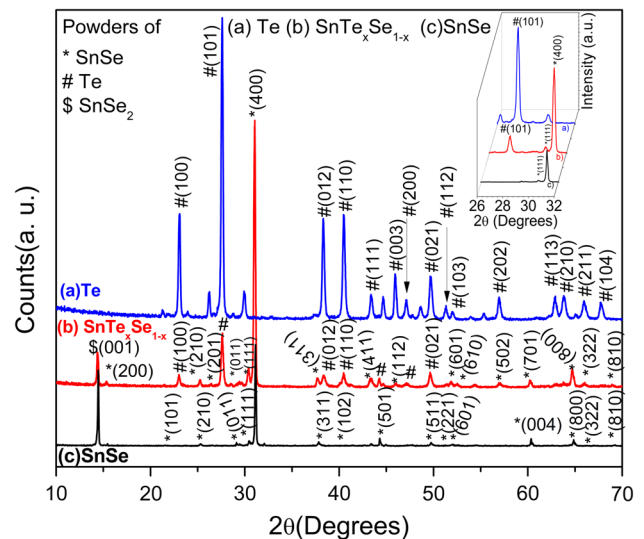Fig. 1. The x-ray diffraction patterns of (a) Te, (b) $SnTe_xSe_{1-x}$ and (c) SnSe powders; magnified 3D views of the peaks from 26° to 32° are presented as inset figure.
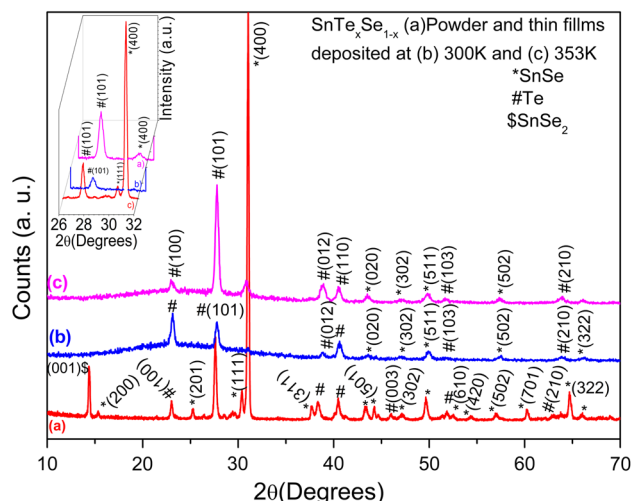
Fig. 2. The x-ray diffraction patterns of SnTe$_x$Se$_{1-x}$ (a) powder, thin films deposited at (b) 300 K and (c) 353 K; magnified 3D views of peaks from 26° to 32° are presented as inset figure.
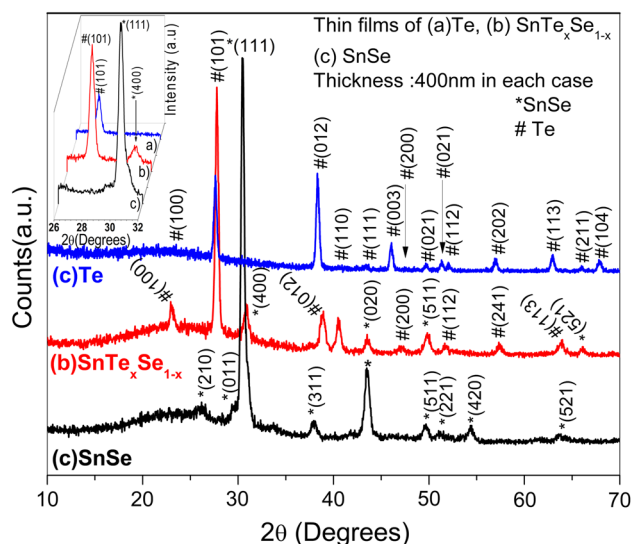

Fig. 3. X-ray diffraction patterns of 400 nm films (a) Te, (b) SnTe$_x$Se$_{1-x}$ and (c) SnSe deposited at 353 K; magnified 3D views of peaks from 26° to 32° are presented as inset figure.

thin films have been calculated by using relations established for hexagonal (Te) and orthorhombic (SnSe) crystal systems, respectively.[14] The z-axis strain (ε_{zz}) values of the unit cells of Te and SnSe lattices have been calculated by using Eq. 1 given as under[15]:

$$\varepsilon_{zz}(\%) = \left(\frac{c - c_o}{c_o}\right) \times 100 \qquad (1)$$

where c is the lattice parameter of strained films calculated from the x-ray diffraction data and c_o is the unstrained lattice parameter of bulk SnSe and Te unit cells. The values of unit cell parameters and strain along the z-axis (ε_{zz}) of the thin films are presented in Table I. The cell parameters of SnSe

and Te constituents of SnTe$_x$Se$_{1-x}$ powder as well as their strain parameters (ε_{zz}) are found close to those of SnSe and Te powders deposited separately. Moreover, the SnSe$_2$ (001) phase existed in SnTe$_x$Se$_{1-x}$ and SnSe powders disappears in the deposited films. It is observed that peaks of SnSe and Te constituents shift towards higher 2θ values to the corresponding peaks of SnSe and Te thin films, the c-parameter values of these unit cells decrease while their strain along the z-axis (ε_{zz}) increases to that of SnSe and Te films deposited separately. These deviations in cell parameters and strain in the lattice of the deposited films may be responsible for the changed characteristics of SnTe$_x$Se$_{1-x}$ films. The average grain size (D) of the most significant peaks of each phase has been calculated using the Debye–Scherrer relation.[16]

SnTe$_x$Se$_{1-x}$ is found to possess (101) Te and (111) SnSe as most significant peaks (MSP) having grain sizes of 119 nm and 28 nm, respectively. These grain sizes, however, are lower than those of corresponding peaks of separately deposited SnSe and Te films. Moreover, MSP of Te constituent is more than three times higher than that of SnSe. The dislocation density (δ), microstrain (ε) and number of crystallites per unit area (N) of the films were calculated by using the relations reported by different authors.[17,18]

The dislocation density [$\delta = 7.181 \times 10^{13}$ lines^{-2}/m^{-4}, Te; 1.32×10^{16} lines^{-2}/m^{-4}, SnSe], microstrain [$\varepsilon = 0.0016$, Te; 0.0025, SnSe] and number of crystallites/area [$N = 2.434 \times 10^{14}$ m^{-2}, Te; 1.923×10^{16} m^{-2}, SnSe] values of Te and SnSe constituents of SnTe$_x$Se$_{1-x}$ are found higher to the corresponding parameters of SnSe ($\delta = 2.456 \times 10^{14}$ lines^{-2}/m^{-4}, $\varepsilon = 0.0018$, $N = 2.456 \times 10^{14}$ m^{-2}) and Te ($\delta = 1.171 \times 10^{13}$ lines^{-2}/m^{-4}, $\varepsilon = 0.0014$, $N = 1.60 \times 10^{13}$ m^{-2}) films. These variations also play a role in the changed characteristics of SnTe$_x$Se$_{1-x}$ films.

Morphological and Compositional Analysis

The scanning electron microscopy (SEM) images of Te, SnTe$_x$Se$_{1-x}$ and SnSe films, each with a thickness of 400 nm deposited at 353 K, are shown in Fig. 4a–c; their magnified images are shown as insets in the respective figures. The Te films show flaky type grains, whereas SnSe has exhibited spherical shapes. The images of SnTe$_x$Se$_{1-x}$ films show mixed effect of modified morphologies of Te and SnSe crystallites. As a result, SnTe$_x$Se$_{1-x}$ films are seen to demonstrate 'flaky-spherical' morphology having structures of hexagonal Te embedded with orthorhombic SnSe. The films exhibit tightly bonded granular structure that occupy pinholes. The arrangement is observed to be uniformly distributed over the entire surface.

The compositions of SnTe$_x$Se$_{1-x}$ powder and thin films deposited at different substrate temperatures varying from 300 K to 553 K have been determined

Table I. Structural parameters of Te, SnTe$_{0.32}$Se$_{0.68}$ and SnSe thin films deposited at 353 K (80°C) substrate temperature

| Material type | 2θ (°) | (hkl) | Cell parameters | | | Axis strain ε_{zz} (%) | | Grain size (nm) | FWHM |
			a (Å)	b (Å)	c (Å)	x-axis	c-axis	D (nm)	B (°)
Te constituent of SnTe$_{0.32}$ Se$_{0.68}$	27.778 (1)	101	4.445	4.445	5.793	0.269	2.294	119	0.379
Te Pure	27.616 (2)	101	4.442	4.442	5.915	0.336	0.236	292.2	0.338
SnSe constituent of SnTe$_{0.32}$ Se$_{0.68}$	30.830 (1)	111	11.549	4.151	4.316	0.450	2.793	28	0.609
SnSe pure	30.487 (3)	111	11.530	4.155	4.427	0.282	0.293	63.80	0.439

JCPDS card no. 89-4899, $a = 4.457$, $b = 4.457$, $c = 5.929$ Å (Te); JCPDS card no. 48-1224, $a = 11.4976$, $b = 4.153$, $c = 4.44$ Å (SnSe); JCPDS card no. 23-0602, $a = 3.810$, $b = 6.140$, $c = 1.6115$ Å (SnSe$_2$).

from EDAX; their respective changes are shown in Table II. The atomic percentage of the elements observed in SnTe$_x$Se$_{1-x}$ powder and thin films at 353 K are plotted in Fig. 5a and b. With reference to our previous work on SnTe$_x$Se$_{1-x}$,[13] the compositions of the constituent materials vary in the deposited films with increase in the substrate temperature from 300 K to 553 K. However, it is observed from this table that alloy formation lacked in SnTe$_x$Se$_{1-x}$ films deposited at room temperature. The EDAX data of these films did not show the presence of Sn at this temperature; moreover, Te content disappears at 453 K and above. The alloy formations of SnTe$_x$Se$_{1-x}$ are confined from 353 K to 453 K having slight variations in composition with change in substrate temperature. Moreover, the atomic compositions of the films deposited at 353 K are found close to that powder material.

Optical Analysis

In order to analyse the optical behaviour of the SnTe$_x$Se$_{1-x}$ thin films, a comparison of transmission (%), absorption coefficient (α) and bandgap (E_g) values of SnTe$_x$Se$_{1-x}$ films deposited at substrate temperature of 353 K is made up with those of separately deposited SnSe and Te films. The transmittance spectra of SnTe$_x$Se$_{1-x}$, Te and SnSe films as measured in the range of 750 nm to 2250 nm (Vis–NIR region) has been shown as inset in Fig. 6. The comparison reveals that SnTe$_x$Se$_{1-x}$ films provide a sharp transition from high to low values in transmission spectra and its transmission percentage values are found falling between those of SnSe and Te.

The absorption coefficient (α) values has been determined from the transmission spectra according to Eq. 2 and their optical bandgaps (E_g) are determined by Tauc's relation as per Eq. 3[18,19]:

$$\alpha = \frac{1}{d}\left(\frac{1}{\ln(T)}\right) \tag{2}$$

$$\alpha h v = A\left(h v - E_g\right)^{1/2} \tag{3}$$

where d, thickness of the thin films; T, transmission percentage; $h v$, the photon energy and E_g, optical bandgap and A, proportionality constant.

The optical absorption coefficient (α) versus photon energy ($h v$) plots of the SnTe$_x$Se$_{1-x}$, Te and SnSe films have been shown in Fig. 6. The plots indicate SnTe$_x$Se$_{1-x}$ to possess absorption coefficient (α, 1.62×10^5 cm^{-1}) value higher than that of SnSe (α, 1.42×10^5 cm^{-1}) and Te (α, 8.2×10^4 cm^{-1}) films. The E_g values of the SnTe$_x$Se$_{1-x}$, Te and SnSe films have been determined from $(\alpha h v)^2$ verses ($h v$) plots by extrapolating the linear part of the curve at $(\alpha h v)^2 = 0$ axis. The E_g values of SnTe$_x$Se$_{1-x}$, Te and SnSe so obtained are shown in Fig. 7a–c; the linearity of these plots indicates the presence of direct bandgap in undertaken semiconductors and the value of SnTe$_x$Se$_{1-x}$ ($E_g = 0.93$ eV) is found to exist in between that of Te ($E_g = 0.73$ eV) and SnSe ($E_g = 1.42$ eV). In order to consider their usage for various optoelectronic applications, it is important to determine the smoothness of the surface of thin films which can be gauged from the extinction coefficient (K) calculated from the equation reported by Beena et al.[20] The variations in the extinction coefficient K values with change in wavelength from 750 nm to 2250 nm for Te, SnTe$_x$Se$_{1-x}$ and SnSe films have been shown in Fig. 8. The K variations of SnTe$_x$Se$_{1-x}$, were found similar to that of SnSe, moreover, the value for SnTe$_x$Se$_{1-x}$ varies from 0.3 to 1.2 with change in the wavelength from 750 nm to 2250 nm with minimum value of 0.3 at 1700 nm. Thus, the SnTe$_x$Se$_{1-x}$ films provide smooth surface which is suitable for optoelectronic device fabrication.

Electrical Characterizations

The electrical properties of SnTe$_x$Se$_{1-x}$, Te and SnSe films deposited at 353 K were studied by
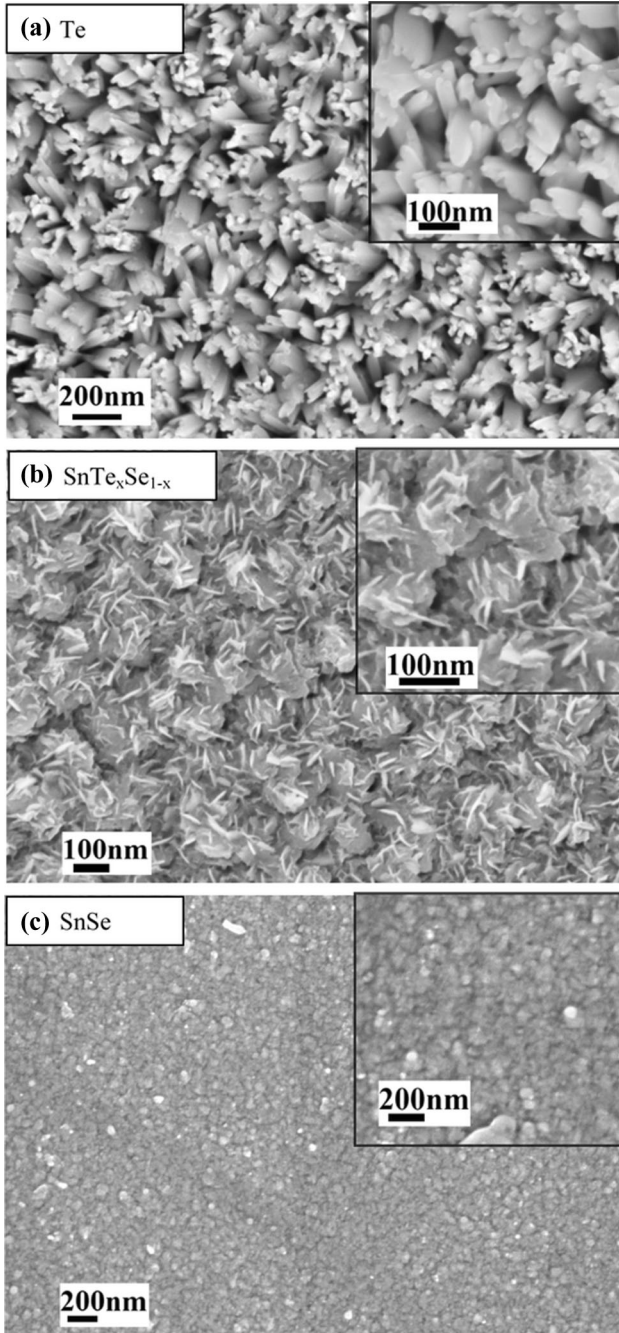
Fig. 4. SEM micrographs of (a) Te, (b) SnTe$_x$Se$_{1-x}$, and (c) SnSe thin film deposited at 353 K; magnified images in each case are presented as inset figures.

vander Pauw method using a Hall measurement setup (Make: BioRad; Model: HL 5200) at room temperature.[21] The films of these materials indicate p-type conductivity.[4] The SnTe$_x$Se$_{1-x}$ films deposited at 353 K provide low resistivity (ρ), moderate mobility (μ) and high carrier concentration (N_A) values. The resistivity value of SnTe$_x$Se$_{1-x}$ films (ρ, $\sim 6.12 \times 10^{-2}$ Ω cm) is found lower to SnSe (ρ, $\sim 1.92 \times 10^4$ Ω cm); carrier concentration (N_A, $\sim 1.31 \times 10^{19}$ cm^{-3}) is higher to SnSe films

Table II. Compositions of SnTe$_x$Se$_{1-x}$ powder and thin films deposited at different substrate temperatures varying from 300 K to 553 K

SnTe$_x$Se$_{1-x}$ alloy	Composition
Powder	SnTe$_{0.68}$Se$_{0.32}$
Thin films at different temperatures	
300 K	No alloy formation
353 K	SnTe$_{0.66}$Se$_{0.34}$
403 K	SnTe$_{0.58}$Se$_{0.42}$
453 K	SnTe$_{0.29}$Se$_{0.71}$
503 K	No alloy formation
553 K	No alloy formation

(N_A, $\sim 6.12 \times 10^{12}$ cm^{-3}), whereas mobility value (μ, ~ 25.8 cm^2/Vs) is comparable to that of SnSe (μ, ~ 37.1 cm^2/Vs) thin films of same thickness. Further, these parameters of SnTe$_x$Se$_{1-x}$ thin films are sensitive to the change in the substrate temperature from 353 K to 453 K due to the changed composition of the films.[13]

Current-Transport Behaviour of Metal/p-SnTe$_x$Se$_{1-x}$ Semiconductor Interface

The most important aspect of semiconductors is the process that determines the flow of electrons over the top of the barrier from semiconductor to the metal and vice versa when bias voltage is applied to the interface. Generally, two types of contacts, viz. ohmic and Schottky, are formed between metal and semiconductor.[22] In order to form an ohmic contact with a semiconductor, the work function of the metal (ϕ_m) must be greater than that of the semiconductor (ϕ_s), whereas the metal–semiconductor (MS) contacts provide rectifying behaviour when the work function of the semiconductor is greater than the metal.[23,24] The aluminium (Al) and indium (In) metals are seen to form ohmic contacts with p-SnTe$_x$Se$_{1-x}$ semiconductors. These contacts exhibit linear and symmetrical behaviour of their I–V characteristics and provide low resistance. Between the two metals used for ohmic contact formation, Al shows lower resistance than In, while the thermally evaporated silver (Ag) dots on p-SnTe$_x$Se$_{1-x}$ semiconductor provide Schottky interface. These diodes show good rectifying behaviour, their I–V characteristics have been analyzed on the basis of thermionic emission and diffusion (TED) theory according to Eqs. 4 and 5:[23]

$$I = AA * T^2 \exp\left[\frac{-q\phi_{Bo}}{kT}\right] \exp\left(\frac{q(V - IR_s)}{\eta kT}\right) \quad (4)$$

where

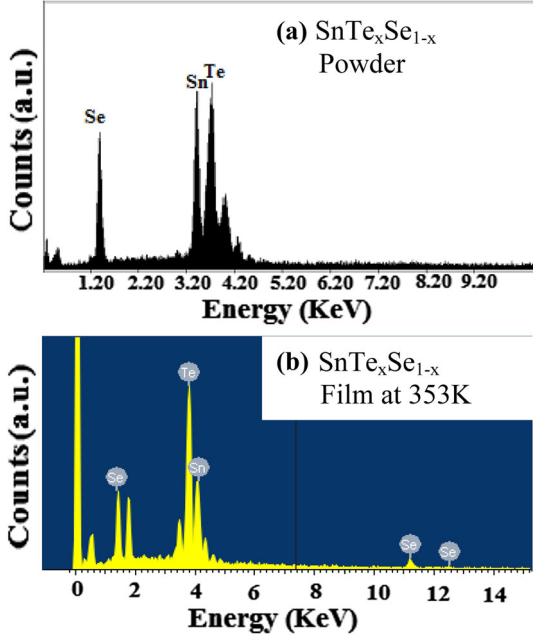$$I_o = AA * T^2 \exp\left[\frac{-q\phi_{Bo}}{kT}\right], \quad (5)$$

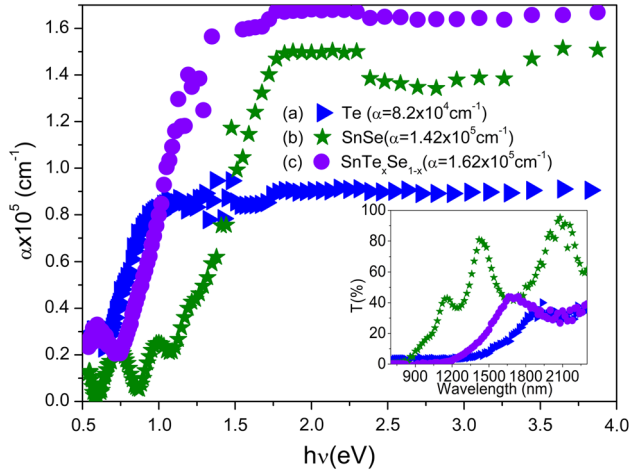Fig. 5. EDAX of the SnTe$_x$Se$_{1-x}$ (a) powder and (b) films deposited at 353 K substrate temperature.

Fig. 7. $(\alpha h\nu)^2$ versus $(h\nu)$ plots of (a) Te (b) SnTe$_x$Se$_{1-x}$ and (c) SnSe films deposited at 353 K.

Fig. 6. Absorption coefficient (α) versus photon energy ($h\nu$) plots of 400 nm SnTe$_x$Se$_{1-x}$ films deposited at 353 K; their transmission response is presented as inset figure.

Fig. 8. Extinction coefficient (K) versus wavelength (λ) plots of (a) Te (b) SnTe$_x$Se$_{1-x}$ and (c) SnSe films each of 400 nm deposited at 353 K.

where V is the applied voltage; q, electronic charge; η, ideality factor; k, Boltzmann constant; T, temperature (in Kelvin); R_s, series resistance; I_o, reverse saturation current; A, diode area; A^*, the effective Richardson constant of the material (18 A cm^{-2} K^{-2} for SnSe is referenced in the present case). The forward and reverse current–voltage (I–V) characteristics of Ag/p-SnTe$_x$Se$_{1-x}$ Schottky diodes formed by evaporating Ag dots with diameters of 1.0 mm, 1.5 mm and 2.0 mm have been shown in Fig. 9.

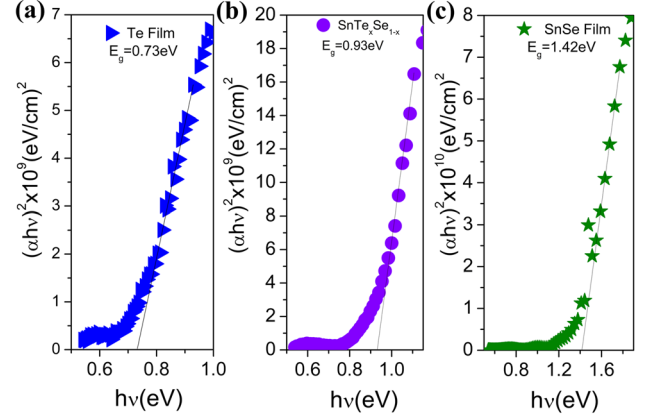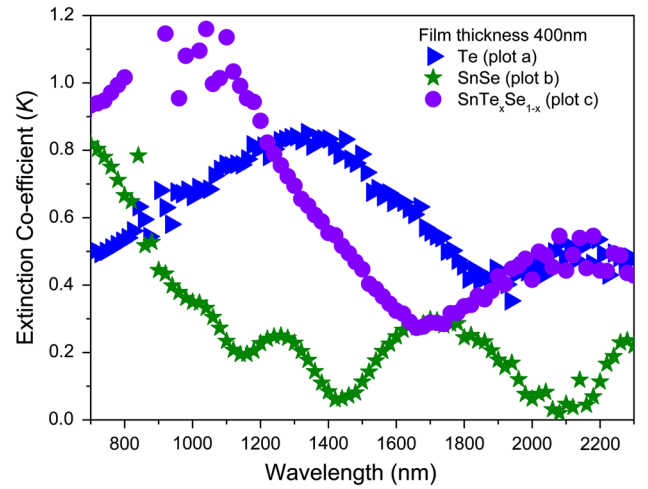The forward log (I)–V characteristics are found linear over three orders of current along y-axis. The

I–V characteristics deviate from straight line at high forward bias (V) due to series resistance (R_S) of the diodes, back contact, and external connections. The values of the ideality factors, barrier heights and series resistances obtained from Eqs. 4 and 5 for diodes having different interface areas have been presented in table form as an inset of Fig. 9. The values of ideality factor (η) decrease from 3.99 to 2.90; series resistance (R_s) of the diodes decrease from 388 Ω to 325 Ω, whereas their zero bias barrier heights (ϕ_{bo}) increase from 0.68 eV to 0.76 eV with increase in the diameter value from 1.0 mm to 2.0 mm. The higher value of ideality factors indicates deviation from thermionic emission and diffusion (TED) current transport mechanism.[25] These changes have been explained on the basis of increased contribution of peripheral current in Schottky diodes with increase in area of the MS interface which provides improvement in the diode parameters.[26]
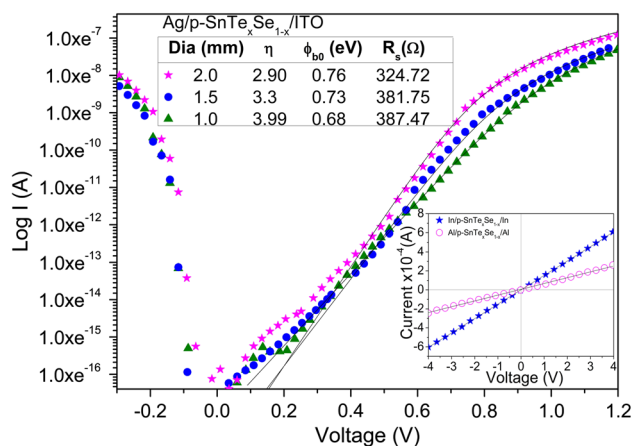
Fig. 9. The forward and reverse current–voltage (I–V) characteristics of Ag/p-SnTe$_x$Se$_{1-x}$ circular Schottky diodes with diameters of 1.0 mm, 1.5 mm and 2.0 mm; the ohmic contacts of Al and In with p-SnTe$_x$Se$_{1-x}$ thin films are shown as inset figures; ideality factors, barrier heights and series resistance values are inserted as inset table.

CONCLUSIONS

The variations in the unit cells parameters and strain in the lattices of SnSe and Te constituents of SnTe$_x$Se$_{1-x}$ have been observed in the films deposited at 353 K to that of SnSe film grown separately. Moreover, the changes in composition of the films have been found to be temperature activation phenomenon. These modifications in the structures have caused variations in the optical and electrical properties of the deposited films; the changes in the corresponding parameters of SnTe$_x$Se$_{1-x}$ show an improvement over SnSe. The current transport over Ag/p-SnTe$_x$Se$_{1-x}$ Schottky diodes exhibited reasonably acceptable rectifying behaviour. Outcome of this study, SnTe$_x$Se$_{1-x}$ thin films are found a suitable alternate to SnSe for optoelectronic device applications.

REFERENCES

1. S. Logothetidis and H.M. Polatoglou, *Phys. Rev. B* 36, 7491 (1987).
2. J.P. Singh and R.K. Bedi, *J. Appl. Phys.* 68, 2776 (1990).
3. R.K. Bedi, B.S.V. Gopalan, and J. Mujhi, in *Physics and Technology of semiconductor Devices and Integrated Circuits SPIE Publs Conference Proceedings* (1992), pp. 104.
4. V. Kumar, P. Kumar, S. Yadav, V. Kumar, M.K. Bansal, and D.K. Dwivedi, *J. Mater. Sci. Mater. Electron.* 27, 4043 (2016).
5. J. Shen, J.M. Woods, Y. Xie, M.D. Morales-Acosta, and J.J. Cha, *Adv. Electron. Mater.* 2, 1600144 (2016).
6. P.R. Manivasan and J. Kim, *Cryst. Eng. Commun.* 17, 807 (2015).
7. B. Subramanium, C. Sanjeeviraja, and M. Jayachandran, *Bull. Electrochem.* 18, 349 (2002).
8. S.V. Eremeev, YuM Koroteev, I.A. Nechaev, and E.V. Chulkov, *Phys. Rev. B* 89, 165424 (2014).
9. L.I. Soliman and B.S. Farag, *Ind. J. Pure Appl. Phys.* 41, 131 (2003).
10. H.A. Zayed, L.I. Soliman, B.S. Farag, and F.M. Shehata, *Ind. J. Pure Appl. Phys.* 30, 654 (2001).
11. S. Ariponnammal, C. Venkateshwaran, and S. Natarajan, *Phys. Stat. Sol. (b)* 197, K1 (1996).
12. L.P. Tan, T. Sun, S. Fan, R.V. Ramanujan, and H.H. Hng, *J. Alloys Compd.* 587, 420 (2014).
13. N. Padha, A. Devi, A. Banotra, S. Kumar, and A. Kumar, *Mater. Res. Exp.* 4, 116311 (2017).
14. B.D. Cullity, *Elements of X-Ray Diffraction*, 2nd ed. (Manila: Addison-Wesley Publishing Company, 1956), p. 501.
15. T. Prasada Rao and M.C. Santhoshkumar, *Appl. Surf. Sci.* 255, 4579 (2009).
16. M. Bicer and I. Sisman, *Appl. Surf. Sci.* 257, 2944 (2011).
17. P. Bindu and S. Thomas, *J. Theor. Appl. Phys.* 8, 134 (2014).
18. M. Devika, K.T.R. Reddy, N.K. Reddy, K. Ramesh, R. Ganesan, E.S.R. Gopal, and K.R. Gunasekhar, *J. Appl. Phys.* 100, 023518 (2006).
19. J. Tauc, R. Grigorovici, and A. Vancu, *Phys. Status Solidi B* 15, 627 (1966).
20. D. Beena, K.J. Lethy, R. Vinodkumar, V.P.M. Pillai, V. Ganesan, D.M. Phase, and S.K. Sudheer, *Appl. Surf. Sci.* 255, 8334 (2009).
21. K.A. Borup, E.S. Toberer, L.D. Zoltan, G. Nakatsukasa, M. Errico, J.-P. Fleurial, B.B. Iversen, and G. Jeffrey Snyder, *Rev. Sci. Instrum.* 83, 122 (2012).
22. M. Wittmer, *Phys. Rev. B* 43, 4385 (1991).
23. E.H. Rhoderick and R.H. Wiliams, *Metal Semiconductor Contacts*, 2nd ed. (Oxford: Clarendon Press, 1988), p. 90.
24. M.S. Tyagi, *Introduction Semiconductor Materials and Devices* (Delhi: Wiley, 2008), p. 270.
25. N. Tugluoglu, S. Karadeniz, M. Sahin, and H. Safak, *Appl. Surf. Sci.* 233, 320 (2004).
26. M.A. Yaganeh, S. Rahmatallahpur, A. Nozad, and R.K. Mamedov, *Chin. Phys. B* 19, 107207 (2010).